

Perfect polar stacking of parallel beloamphiphile layers. Synthesis, structure and solid-state optical properties of the unsymmetrical acetophenone azine DCA†

Rainer Glaser,^{*a} Nathan Knotts,^a Ping Yu,^{*b} Linghui Li,^b Meera Chandrasekhar,^{*b} Christopher Martin^b and Charles L. Barnes^c

Received 8th November 2005, Accepted 8th February 2006

First published as an Advance Article on the web 2nd May 2006

DOI: 10.1039/b515739k

Extraordinary high degrees of polar order can be achieved by a rational design that involves the polar stacking of parallel beloamphiphile monolayers (PBAM). This strategy is exemplified by the acetophenone azines MCA (4-methoxy-4'-chloroacetophenone azine) and DCA (4-decoxy-4'-chloroacetophenone azine). The beloamphiphile design aims to achieve strong lateral interactions by way of arene–arene, azine–azine, arene–azine and halogen-bonding interactions. Dipole-induced interactions and halogen bonding dominate interlayer interactions and halogen bonding is shown to effect the layer stacking. Crystals of DCA contain PBAMs with perfect polar order *and* perfect polar layer stacking, while crystals of MCA features perfect polar order only in one of two layers and layer stacking is polar but not entirely perfect. We report the synthesis of the beloamphiphile DCA, its crystal structure, and we present a comparative discussion of the structures and intermolecular interactions of MCA and DCA. Absorbance and photoluminescence measurements have been carried out for solutions of DCA and for DCA crystals. DCA exhibits a broad emission centered at 2.5 eV when excited with UV radiation. The nonlinear optical response was studied by measuring second harmonic generation (SHG). Strong SHG signals have been observed due to the polar alignment and the DCA crystal's NLO response is 34 times larger than that of urea. Optimization of the beloamphiphile and systematic SAR studies of the polar organic crystals, which are now possible for the very first time, will further improve the performance of this new class of functional organic materials. The materials are organic semiconductors and show promise as blue emitters, as nonlinear optical materials and as OLED materials.

Introduction

Polar order in the biosphere is limited to nanometer-sized domains, occurs with essentially complete cancellation, or is avoided on purpose. One thus wonders whether large-scale polar order is even possible and this question is the subject of the dipole alignment problem.¹ We have addressed this challenge with an interdisciplinary approach and a rational design that aims at the polar stacking of parallel beloamphiphile monolayers (PBAM).^{2,3}

The thoughts “lipid bilayer” and “contains oppositely oriented layers” are tightly chunked and one is thus not likely to even consider lipid bilayers an inspiration for the construction of polar order. There exists a deep chasm between common ideas of nicely organized layers and the reality of bilayers⁴ and this realization might further discourage the search for polar order in this domain. The lipid bilayer energetics in water is largely driven by the desire

of the polar head groups to interact with each other and with water,^{5,6} and the lipophilic moieties merely “get out of the way.” It is important to stress the “and with water” part of the statement and to realize that this is one of the major reasons for the opposite orientation of the layers in a lipid bilayer.

Here we discuss aspects of interlayer control in the construction of polar crystals by polar PBAM stacking. The design ideas are exemplified by the closely related acetophenone azines MCA (4-methoxy-4'-chloroacetophenone azine, a.k.a. the (MeO,Cl)-azine) and DCA (4-decoxy-4'-chloroacetophenone azine, a.k.a. (DecO,Cl)-azine). These beloamphiphiles are ascendants of a new generation of highly anisotropic functional materials with perfect polar order. The materials are organic semiconductors and show promise as blue-emitters, as nonlinear optical materials and as OLED materials.

Polar order based on beloamphiphiles

Amphiphiles are formed by combination of a polar, water-soluble head group and a nonpolar and water-insoluble alkyl chain. Idiotoamphiphiles and bolaamphiphiles, respectively, contain two identical or two different head groups, respectively, at the ends of a nonpolar chain. Beloamphiphiles are polar and conjugated bolaamphiphiles. In particular, symmetric D–D and A–A

^aDepartment of Chemistry, University of Missouri-Columbia, Columbia, Missouri, 65211, USA. E-mail: glaser@missouri.edu

^bDepartment of Physics and Astronomy, University of Missouri-Columbia, Columbia, Missouri, 65211, USA. E-mail: yuping@missouri.edu, meerac@missouri.edu

^cElmer O. Schlemper X-ray Diffraction Center, University of Missouri-Columbia, Columbia, Missouri, 65211, USA

† Based on the presentation given at Dalton Discussion No. 9, 19–21st April 2006, Hulme Hall, Manchester, UK.

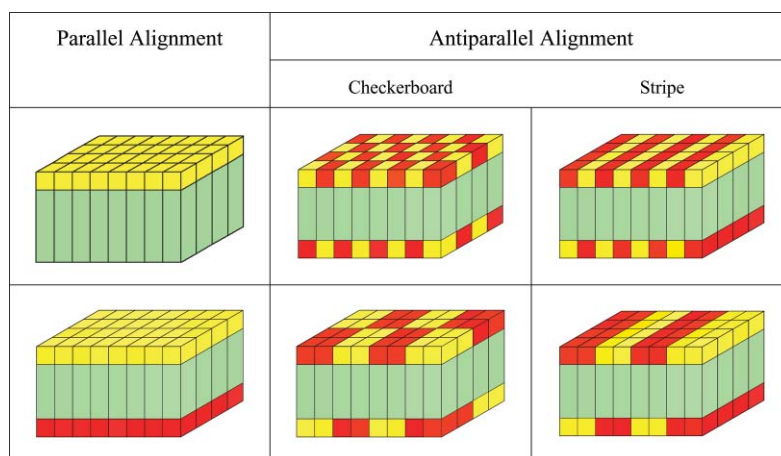


Fig. 1 Parallel amphiphile and belowamphiphile monolayers (PAM and PBAM) are shown on the left. Antiparallel belowamphiphile monolayers (APBAM) are realized with checkerboard and stripe motifs and two examples are shown of each. Color key: Head groups in red and yellow, spacers in green.

substituted (conjugated) molecules are idioteloamphiphiles while D–A, D1–D2 and A1–A2 substituted (conjugated) molecules are belowamphiphiles. Some important amphiphile monolayers are shown in Fig. 1.

The monolayers are classified as “parallel” or “antiparallel” depending as to whether all amphiphiles are oriented in the same direction or whether their orientations alternate in at least one direction. While there is *one* polar monolayer, nonpolar monolayers can be constructed *in a great many ways* and the checkerboard and stripe motifs are common. The majority of layer-forming amphiphiles crystallize with alternating orientation in both layer directions (checker-board) and even polar alignment in one layer direction (stripe) is rare. Polar order throughout an amphiphile monolayer apparently was first observed in crystals of 11-aminoundecanoic acid hydrobromide hemihydrate.⁷ Crystals of Sim’s acid contain “normal bilayers” and are overall nonpolar. The crystal structure of a 1-galactosamide with a tethered carboxylic acid was reported in 2001 as the first case of polar stacking of polar belowamphiphile monolayers.⁸ As part of our analysis of the polar (MeO,COMe)-biphenyl,⁹ we explained the polar structures of the (*n*Bu,CN)- and (Me₂N,CN)-biphenyls reported by Haase¹⁰ in 1987 and by Zyss¹¹ in 1991, respectively, as the result of polar stacking of polar belowamphiphile monolayers. In addition, a handful of other molecular materials and of organic salts are known that crystallize with polar order. We cited these materials elsewhere^{2,12} and pointed up that they vary greatly in their constitutions, that they all were discovered by different groups, and that none of these discoveries has subsequently resulted in conceptualization, repetition or refinement. Belowamphiphile design for the achievement of perfect polar stacking of parallel belowamphiphile monolayers (PBAMs) is shown in Fig. 2.

Studies of point dipole lattices showed, as expected, that an antiparallel alignment is always preferred over the parallel aligned lattice and, to our surprise, that the latter might be a local minimum.^{13,14} Hence, a systematic solution of the dipole-alignment problem was possible and the study provided guidance. Conjugated D–A systems were sought with modest dipole moments along their long axes and with the propensity for high lateral intermolecular interactions.¹⁵ The placement of two acceptors with opposite polarity in the center of the molecules achieves the design

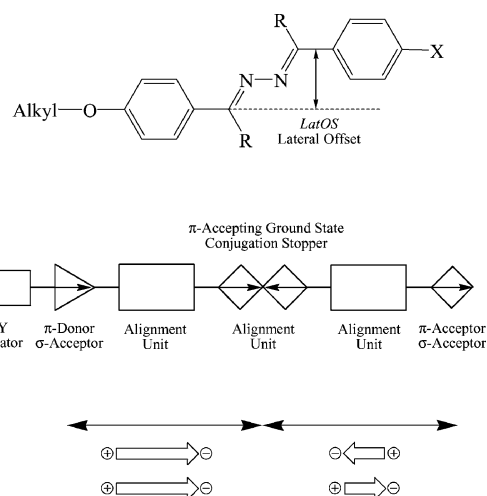


Fig. 2 Belowamphiphile design for the achievement of perfect polar stacking of parallel belowamphiphile monolayers (PBAMs).

goal of “dipole minimization” and we have demonstrated this concept to be true.^{16–18} The design minimizes through-conjugation in the ground state with the result that one half of the molecule remains dipolar while the other half is rendered quadrupolar along the long axis. The design employs arenes as “alignment units” and relies on lateral arene–arene attractions (Ar ··· Ar).¹⁹ The Q_{zz} component of the azine moiety is largely due to the π -system and compares on a per electron basis with Q_{zz} of benzene. The azine moiety thus engages in strong lateral quadrupole–quadrupole interactions with neighboring azine moieties (Az ··· Az) and with arenes (Az ··· Ar).²⁰ Finally, the interactions between the head groups X and Y contribute to *both* intra- and interlayer interactions. The interactions between head groups often involve halogen bonding either between two halogens or between halogen atoms (I, Br, Cl) and N- or O-atoms.²¹

$${}^{\text{intra}}E_{\text{pp}} = E(\text{X1} \cdots \text{X2}) + E(\text{Ar}_X1 \cdots \text{Ar}_X2) + E(\text{Az1} \cdots \text{Az2}) + E(\text{Ar}_Y1 \cdots \text{Ar}_Y2) + E(\text{Y1} \cdots \text{Y2})$$

$${}^{\text{intra}}E_{\text{app}} = E(\text{X1} \cdots \text{Y2}) + E(\text{Ar}_X1 \cdots \text{Ar}_Y2) + E(\text{Az1} \cdots \text{Az2}) + E(\text{Ar}_Y1 \cdots \text{Ar}_X2) + E(\text{Y1} \cdots \text{X2})$$

$${}^{\text{inter}}E_{\text{pp}} = E(\text{X1} \cdots \text{Y2}) + E(\text{Y1} \cdots \text{X2})$$

$${}^{\text{inter}}E_{\text{app}} = E(\text{X1} \cdots \text{X2}) + E(\text{Y1} \cdots \text{Y2})$$

The intra- and interlayer interactions energies E_{pp} and E_{app} , respectively, between pairs of parallel- or antiparallel molecules, respectively, differ in an essential manner in how they are effected by pure ($\text{X} \cdots \text{X}$ and $\text{Y} \cdots \text{Y}$) and mixed ($\text{X} \cdots \text{Y}$) terms and suggest that the driving forces for layer formation and layer stacking are in opposition. Pure pair interactions favor parallel alignment in layers while they reduce interlayer binding while mixed interactions favor antiparallel alignment in layers but provide for better interlayer interactions. To succeed in the fabrication of polar order, one must pinpoint this balance: intralayer lateral interactions should be just large enough to make polar layers while still allowing polar stacking of the layers!

We synthesized and crystallized a variety of (Y,X)-azines $\text{Y-Ph-MeC=N-N=CMe-Ph-X}$. Our first success came in 1995 with the (MeO,Br)-azine²² (MBA) and in 2000 we reported the polar structures of the (MeO,Cl)-²³ and (MeO,I)-azines²⁴ (MCA and MIA). Recent efforts have focused on (Y,Hal)-azines with $\text{Y} = \text{EtO}$, PrO , ..., DecO ²⁵ and PhO .²⁶ We also studied a variety of (X,X)-azines ($\text{X} = \text{CH}_3$,²⁷ H ,^{28,29} and others^{30,31}). The present study focuses on an azine with perfect polar order, namely 4-decoxy-4'-chloroacetophenone azine (DCA). The perfect polar order of (DecO,Cl)-azine was determined by single-crystal X-ray diffraction and its optical properties were measured in solution and in crystals.

Probing interlayer interactions in polar crystals

Control of the interlayer bonding region. The (MeO,Hal)-azines share a common crystal architecture and they differ in interesting details. Crystals of the (MeO,I) and (MeO,Br)-azines contain *one* and *two* independent molecules, respectively, but both contain *one* kind of polar layer. The (MeO,Cl)-azine features *four* independent azines and *two* kinds of layers. Each layer of MCA

contains two independent molecules, much like an MBA layer, but only one layer is perfectly aligned while the next features reproducible orientational disorder in one of the two molecules (Fig. 3). The subtle disorder provides a glimpse at the complexity of the interrelation between the choice of the head groups, crystal structure and crystal growth and thereby reveals in a compelling fashion the importance of interlayer communication in all these crystals.

We found that the directionality of the interlayer halogen bonding (Fig. 4) effects the layer stacking of the (MeO,Hal)-azines. This insight suggested that the replacement of the MeO group by the larger DecO group and the avoidance of directional halogen bonding might optimize the overall electrostatic interaction in the stacking direction. We synthesized and crystallized the (DecO,Cl)-azine and, indeed, this azine features perfect polar order in every layer *and* also perfect polar PBAM stacking (Fig. 4). As with MCA and MBA, the unit cell of DCA contains two independent molecules and it remains to be understood why MIA contains just one symmetry independent molecule.

4-Decoxyacetophenone was synthesized by Williamson ether synthesis³² and 4-chloroacetophenone is commercially available. The unsymmetrical azine-coupling employed the phosphorohydrazidate chemistry developed by Zwierzak and co-workers^{33,34} and based on Wadsworth–Emmons type chemistry.²⁵

Longitudinal offset and layer stacking. The monolayers of Fig. 1 are idealized and in reality neighboring molecules may show longitudinal offsets along the long molecular axis (*LonOS*) in one or both layer directions. If the longitudinal offset is modest, the layer is said to remain “flat” (Fig. 5). The polar azines exhibit longitudinal offsets but they are modest and the layers remain flat. While the long axes of the amphiphiles in an ideal-flat layer are perpendicular to the layer surfaces, the longitudinal offset causes the molecules to be inclined and this is illustrated in Fig. 5.

The presence or absence of longitudinal offset determines whether there are options for the layer stacking. The polar stacking

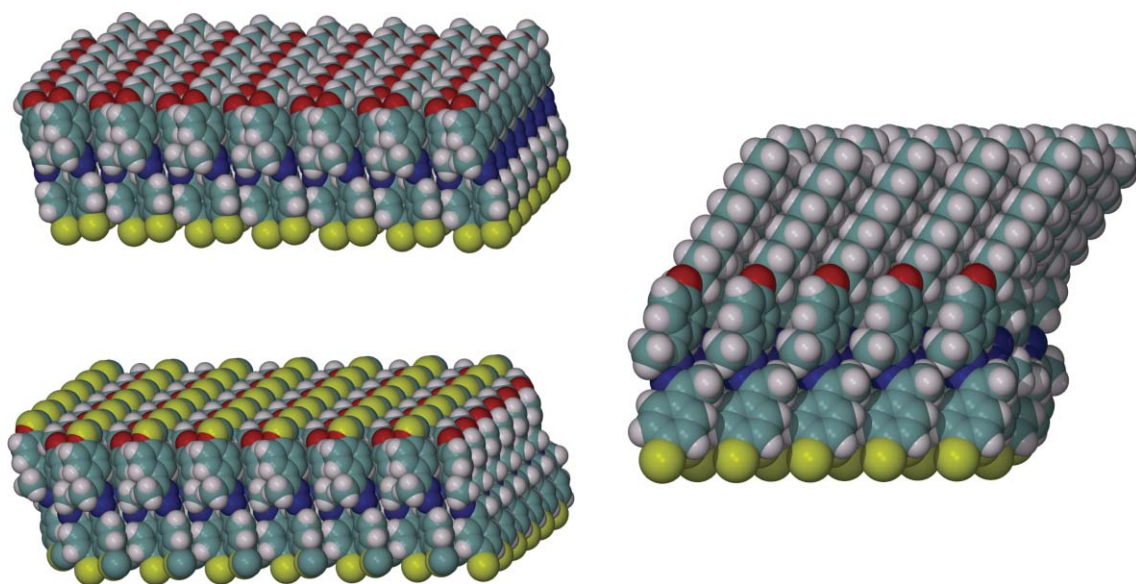


Fig. 3 Parallel beloamphiphile monolayer (PBAM) of (MeO,Cl)-azine (left-top), antiparallel beloamphiphile monolayer (APBAM) of (MeO,Cl)-azine (left-bottom) and parallel beloamphiphile monolayer of (DecO,Cl)-azine (right).

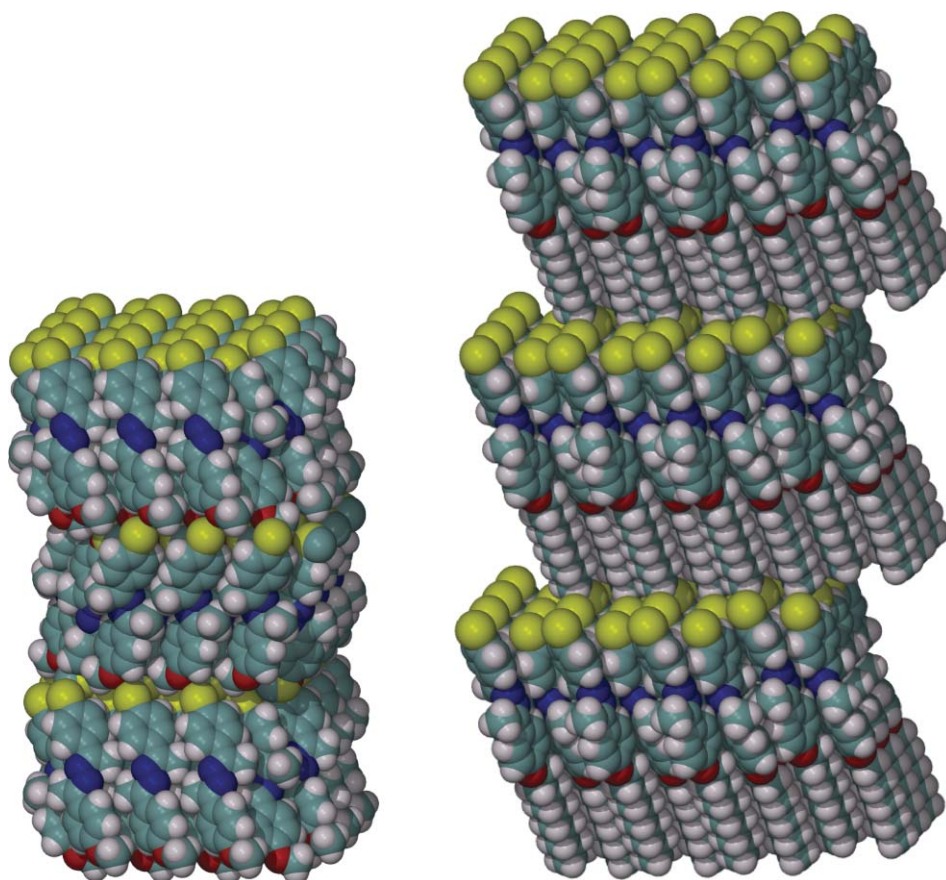


Fig. 4 Polar stacking in (MeO,Cl)-azine (left) and (DecO,Cl)-azine. The azines form perfectly parallel beloamphiphile monolayers and PBAMs stack with polar order. In (MeO,Cl)-azine, directed MeO...Cl interlayer halogen bonding results in near-perfect polar stacking. Such RO...Cl halogen bonding is impossible in the (DecO,Cl)-azines and perfectly polar stacking results.

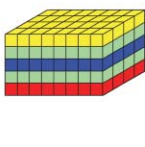
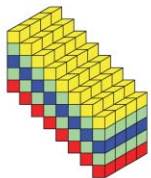
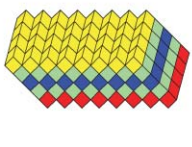
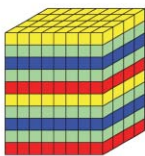
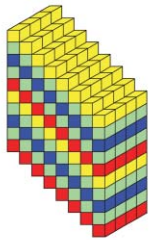
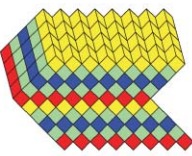
Polar Parallel Beloamphiphile Monolayers (PBAMs)		
Ideal-Flat	Flat	
Nonalternating no longitudinal offset	Nonalternating single-stripe longitudinal offset	
		
Polar PBAM Stacking		
Perfect	Perfect	Near-Perfect
		

Fig. 5 Longitudinal offsets in polar PBAMs gives rise to the possibility of perfect and near-perfect polar stacking. Near-perfect polar stacking occurs in (MeO,Cl)-azine while perfect stacking is realized in the (DecO,Cl)-azine.

of ideal-flat PBAMs must result in perfect polar alignment (or in complete cancellation), while the stacking of flat PBAMs may give either perfect or near-perfect polar alignment in the stacking direction. All of these options are illustrated in Fig. 5.

If there is a choice between near-perfect and perfect stacking, the outcome will depend on surface features. Intrinsically, the polar stacking should be preferred because it optimizes the electrostatic dipole-dipole attraction between the layer polarizations. Hence, the difference in the stacking of MCA and DCA can be rationalized very well. The flat layers of DCA stack with perfect polar order because the layers are held together by dispersion forces. On the other hand, MCA stacks with near-perfect polar order because of directional RO...Cl halogen bonding.

Head groups: layer- and chromophore-maker. In the discussions of MCA, we have usually discussed the methoxy group as head group Y. DCA suggests that it might be advantageous to differentiate between the functions of Y more clearly. It is the primary purpose of Y to contribute to the dipolarity of the molecule and to provide function to the beloamphiphile (*e.g.* optical properties). It is the second purpose of Y to contribute to lateral interactions to enable layer BAM formation. And, finally it is the third purpose of Y to provide interlayer interaction. The last two issues essentially address the anisotropy of interactions involving Y. For the methoxy group, both the O-atom and the

methyl group are available and participate in intra- and interlayer interactions. The situation is very different for the decoxy group. While the O-atom and the alkyl groups both participate in lateral interactions, the O-atom is now completely precluded from participation in interlayer interactions. It is for this reason that we show head group Y in Fig. 2 as consisting of the functional part, the “ π -donor, σ -acceptor” part and of a structure-making part, the “X–Y spacer” part. In Fig. 6, we illustrate schematically a PBAM and a double layer with perfect polar stacking for this case.

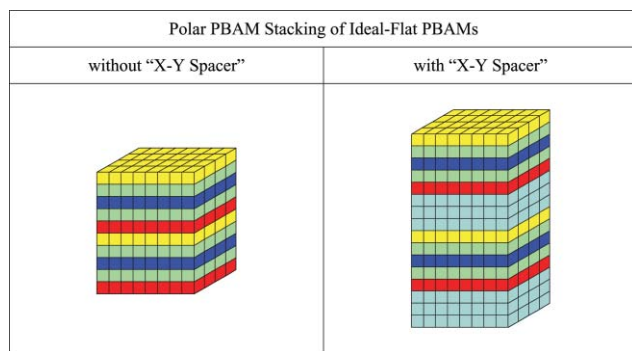


Fig. 6 Separation of the chromophore-maker and the layer-maker functions. The “X–Y Spacer” avoids interlayer interactions between the chromophore-makers.

Lateral offsets, twists and double T-contacts. Azines provide for *lateral offset* (*LatOS*), that is, the local C_2 axes of the *para*-substituted arenes do not coincide (Fig. 2). The lateral offset has major consequences for the crystal architecture: it is responsible for the occurrence of two types of double T-contacts² and for the anisotropy of the strengths of each of these contacts.³

Twists about the N–N and C–Ph bonds causes the two arenes to be nearly perpendicular in acetophenone azines. This conformation enables the azine to engage in four “double T-contacts” of the (ef|fe)- or (fe|ef)-type.³⁵ For a pair of diarenes, the (12|34)-abbreviation specifies for each arene whether it acts as “face” or “edge” in a T-contact, (12| refers to one molecule and |34) to the other, and it is understood that arene 1 interacts with arene 3 and arene 2 with arene 4. Each azine engages in two types of (ef|fe) contacts and the “open” and “closed” contacts are exemplified in Fig. 7. Open and closed contacts alternate in both layer directions.

Polar order and functional organic materials

Absorption and photoluminescence. Absorption and photoluminescence (PL) studies were conducted on a 19.0 μM solution of DCA. Absorption was measured on a Shimadzu UV-2401 PC UV-Vis spectrophotometer from 600 to 200 nm on a sample of 1 cm path length. PL measurements were measured on a Shimadzu RF-5301 PC spectrofluorometer using several excitation wavelengths between 340 and 440 nm in 10 nm increments. Spectra of thin crystalline samples were measured using an Ocean Optics spectrometer, excited by the UV lines of an Ar^+ laser. The crystals were not oriented.

Fig. 8 shows the spectra for the solution and an unoriented crystalline sample. The main absorption peak (solution, dashed line) occurs at 295 nm with a molar absorptivity of 6.41×10^4

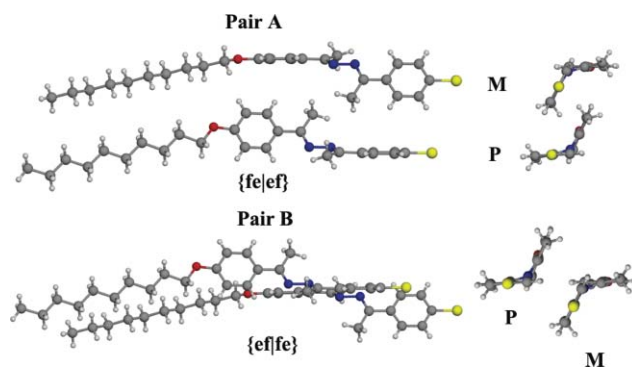


Fig. 7 Double (ef|fe) T-contacts are the layer-making lateral synthon and these contacts can be either “closed” (top) or “open”. Both contacts involve one *P* and one *M* enantiomer. Each azine engages in two closed and two open pair interactions. Decyl groups omitted the Newman perspectives for clarity.

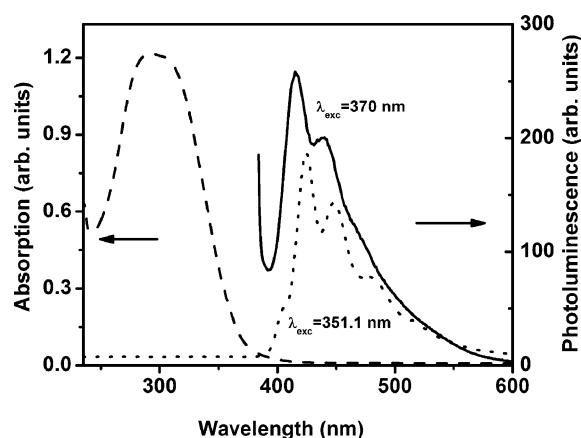


Fig. 8 Absorption (dashed line) and photoluminescence (PL, solid line) spectra of DCA solution and PL spectrum (dotted line) of unoriented DCA crystals. The rising low-wavelength edge of the PL spectrum is due to the exciting radiation. The peaks in the PL are due to the vibronic progression.

as calculated from Beer’s Law. The absorption peak is broad and tailing of the peak occurs past 400 nm. The PL spectrum for the solution (solid line) using the 370 nm excitation is also shown in Fig. 8. A strong peak is observed at 416 nm with a shoulder at 440 nm. The rising edge on the short wavelength side of the PL is due to the exciting radiation. The spectrum of the crystalline sample (dotted line) is similar to that of the solution, however, the peaks are shifted to slightly lower energies and they are better defined. As is typical of many molecular PL spectra, multiple bands due to vibronic progressions associated with the HOMO–LUMO transition^{36,37} are observed. The positions of the peaks are listed in Table 1, from which we deduce an average vibronic

Table 1 PL vibronic peak positions observed for an unoriented DCA crystal

Peak	Excitation at 351.1 nm
0–1	426.7
0–2	449.3
0–3	482.9
0–4	516.3

separation of 0.17 ± 0.02 eV. We note that in the solid state the 0–0 zero-phonon vibronic level is observed only as a weak shoulder on the high energy side near 400 nm, which is consistent with the separations between the vibronics. Ideally one expects a 0–0 peak to be more intense than subsequent vibronics. However, this is true only in very thin samples (usually thin films). In thicker samples, an emitted 0–0 photon can be absorbed by molecules in the path of the photon, which quenches PL from this peak. The overlap between the absorption and the PL spectra determines the efficiency of this self-absorption. In the experimental setup used, crystals were irregular in thickness and spots with different thicknesses were probed with the laser beam. The spectrum in Fig. 8 could be obtained from several thin spots, however, no spot was thin enough to allow the 0–0 transition to be observed.

It is evident from these spectra that little or no absorption occurs at wavelengths longer than 450 nm. The presence of the PL also verifies the absence of absorption beyond 425 nm. Thus the zero-absorption approximation made in order to determine the refractive indices at 532 and 1064 nm (*vide infra*) are valid.

Linear and nonlinear optical properties of DCA crystals

Experiments. The second harmonic generation (SHG) has been measured with the Maker-fringes technique.³⁸ We combine polarization measurements with the results from the Maker-fringe experiments to determine the second-order tensor.

The experimental setup for the SHG measurements in the transmission mode is shown in Fig. 9. The fundamental radiation is provided by a Q-switched Nd:YAG laser at a wavelength of 1.064 microns, with a pulse width of 9 ns and a repetition rate of 25 Hz. The intensity of the fundamental radiation is adjusted by a combination of a half-wave plate and polarizer P1. A second half-wave plate is used to select the angle of the polarized fundamental radiation. The beam is focused to a spot of approximately 30 μm in diameter on the sample surface. A RG715 long-pass filter F1 is placed before the sample to remove any SHG produced by the optical elements in the path before the sample. The SHG signal is detected by a photomultiplier tube. A band-pass filter (BG39) and an interference narrow-band-pass (532 nm) filter are mounted in front of the detector to remove the fundamental radiation.

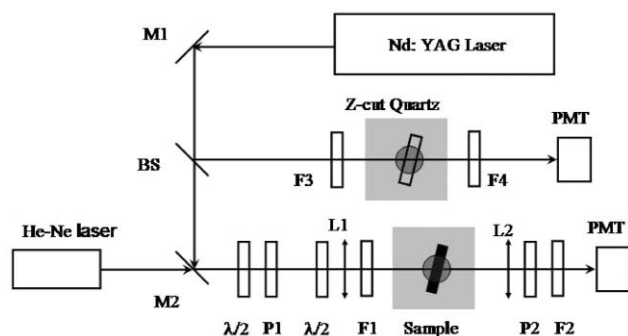


Fig. 9 Experimental setup for SHG measurements. M1 and M2, mirrors reflected at 1064 nm; BS, 50% beam splitter, $\lambda/2$, half-wave plate; P1 and P2, polarizers, L1 and L2, lenses; F1 and F3, long pass filter; F2 and F4, band pass filter, and PMT, photomultiplier tube.

The sample is mounted on a rotational stage in combination with a two-dimensional stage. This mounting allows for the

rotation of the sample around an axis perpendicular to the fundamental radiation beam while maintaining the rotational axis through the sample center. This combined stage is mounted on another three-dimensional translational stage to place the sample at the focal point of the fundamental beam.

One of the experimental difficulties with SHG measurements with a low pulse repetition rate Nd:YAG laser relates to the stability of the laser on a pulse-to-pulse basis.³⁹ In order to remove intensity fluctuations of the fundamental beam, we use a two-beam setup for the simultaneous measurements of SHG from the sample and a Z-cut quartz reference sample (Fig. 9).

Refractive index determination. The linear refractive indices are critical to determining the nonlinear coefficient in the Maker-fringes technique. Various methods have been developed^{40–42} and they include the Abbe refractometer, the Becke-line method, the method of minimum deviation, and the Brewster angle technique. Unfortunately, none of these techniques can be used for our sample due to relatively small size of the organic crystals. Instead, we use a home-made spectrometer that can measure the transmission spectrum with a small beam size of 30 μm . Measurements of refractive index of the sample are based on the following formula if we only count the reflection from two interfaces between the crystal and air:⁴³

$$n(\lambda) = \frac{2 - \sqrt{T(\lambda)} + 2\sqrt{1 - \sqrt{T(\lambda)}}}{\sqrt{T(\lambda)}} \quad (1)$$

The experiments are performed carefully to avoid any scattering from the surface and distortion due to the crystal. According to absorption measurements, the absorption band has a peak at 295 nm and its tail extends to about 415 nm. Since there is no absorption band between 532 and 1064 nm (*vide supra*), our method will give relatively accurate refractive indices at the fundamental and the SHG wavelengths.

Second-order nonlinear optical properties. The crystal structure of DCA has $P1$ symmetry. The relationship between the second-order polarization and the electric field of the fundamental radiation can be written as⁴⁴

$$\begin{bmatrix} P_x \\ P_y \\ P_z \end{bmatrix} = \epsilon_0 \begin{bmatrix} d_{11} & d_{12} & d_{13} & d_{14} & d_{15} & d_{16} \\ d_{16} & d_{22} & d_{23} & d_{24} & d_{14} & d_{12} \\ d_{15} & d_{24} & d_{33} & d_{23} & d_{13} & d_{14} \end{bmatrix} \begin{bmatrix} E_x^2 \\ E_y^2 \\ E_z^2 \\ 2E_y E_z \\ 2E_x E_z \\ 2E_x E_y \end{bmatrix} \quad (2)$$

where E_x , E_y and E_z are the fundamental electric fields, d_{ij} are the second-order nonlinear coefficients and ϵ_0 is the permittivity of free space. We define the laboratory coordinate system to be xyz and the crystal coordinate system to be XYZ as shown in Fig. 10. To separate the d coefficients, we perform experiments with different incident angles of the fundamental radiation. In addition, the polarized fundamental wave is rotated by using the half-wave plate. An analyzer after the sample defines S (perpendicular to the incident plane of the fundamental radiation) and P (parallel to the incident plane) orientations of the harmonic wave.

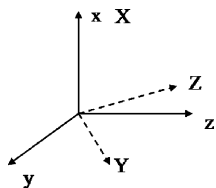


Fig. 10 Relation of the laboratory (xyz) and the crystal (XYZ) coordinate systems. The coordinate systems are used in the calculation of d_{eff} .

At 0° incident angle, the crystal and laboratory coordinate systems coincide. The relationship between the induced second-order polarization and the applied electric field can be written as

$$P_y = \epsilon_0(d_{16} \cos^2 a + d_{22} \sin^2 a + 2d_{12} \cos a \sin a)E^2 \quad (3a)$$

$$P_x = \epsilon_0(d_{11} \cos^2 a + d_{12} \sin^2 a + 2d_{16} \cos a \sin a)E^2 \quad (3b)$$

where a is the angle of the fundamental electric field respect to the x direction in the x - y plane of the laboratory coordinate system. At an incident angle of 45° , the relationship between the induced

second-order polarization and the applied electric field can be written as

$$P_x = \epsilon_0[0.5d_{11} \cos^2 a + 0.5(d_{12} + d_{13} + d_{14})\sin^2 a + (d_{15} + d_{16})\cos a \sin a]E^2 \quad (4a)$$

$$P_y = P_y \cos 45^\circ - P_z \sin 45^\circ \\ = \epsilon_0[0.5(d_{16} - d_{15})\cos^2 a + 0.5(d_{22} + d_{33} - 2d_{14} - 2d_{23})\sin^2 a + (d_{12} + d_{13})\cos a \sin a]E^2 \quad (4b)$$

The measured SHG intensity is shown in Fig. 11 and 12 as the fundamental radiation is rotated 360° in the x - y plane. Compared to the theoretical curves calculated from eqn (3) and (4), we conclude that $d_{22} = 4d_{16}$ and d_{11}, d_{12}, d_{13} are ≈ 0 . The experiments show that d_{22} has the highest value.

Maker-fringes. The measurements of Maker-fringes were performed with the configuration to determine d_{22} at 1064 nm where the organic crystal is rotated in the y - z plane. A typical plot of the Maker-fringes is shown in Fig. 13. The nonlinear coefficients were calibrated with similar data from Z-cut quartz.^{44,45} Since we cannot polish the surface of our sample, the observed minima are nonzero due to the relatively low surface quality as

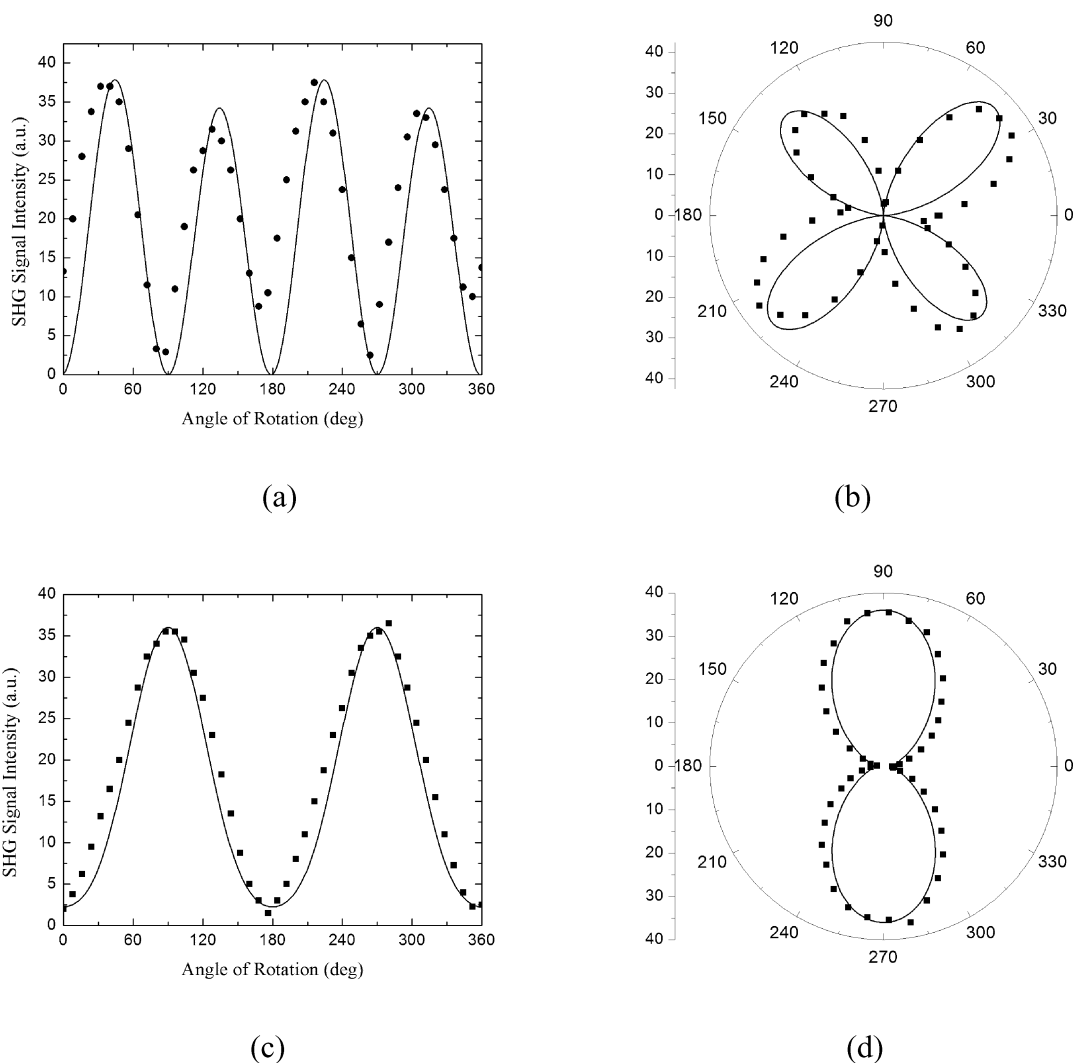
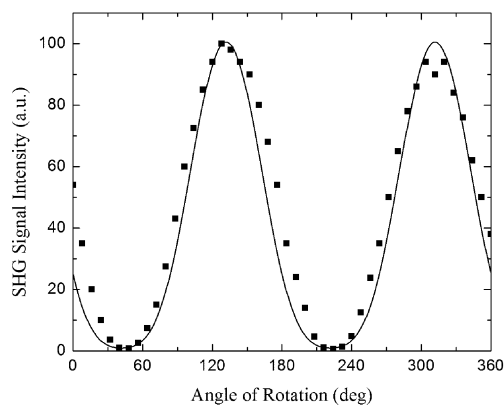
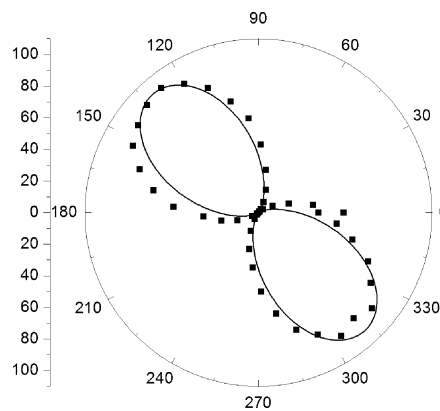


Fig. 11 SHG intensity as a function of a at 0° incident angle. (a) and (b): S component. (c) and (d): P component.



(a)



(b)

Fig. 12 SHG intensity as a function of α at 45° incident angle. S component.

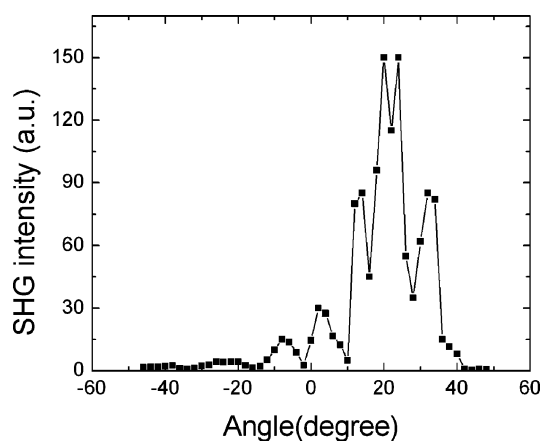


Fig. 13 Maker-fringes under configuration for d_{22} of the DCA crystal.

compared to inorganic materials with harder polishable surfaces (e.g. quartz).

For the organic crystal and quartz, SHG intensity is given by^{46,47}

$$I(2\omega) \propto \frac{l_c^2 I^2(\omega) d_{\text{eff}}^2 \sin^2\left(\frac{\pi l_s}{2l_c}\right)}{n^2(\omega)n(2\omega) \left(\frac{\pi l_s}{2l_c}\right)^2} \quad (5)$$

where $I(\omega)$ is the intensity of the fundamental radiation, d_{eff} is the effective second harmonic coefficient, $n(\omega)$ is the refractive index of the sample at the fundamental radiation wavelength, $n(2\omega)$ is the refractive index at the second harmonic generation wavelength.

The coherence length l_c can be calculated according to $l_c = \lambda/4(n_{2\omega} - n_\omega)$ at a normal incidence, where λ is the wavelength of the fundamental radiation. The length of the sample depends on the incident angle, $l_s = d/\cos\theta$ where d is the thickness of the sample. Table 2 lists the parameters of the sample according to the results from the linear optical properties. As can be seen from Table 2, the coherence length is relatively short for this sample. This explains the difficulty in getting good zeros for the Maker-fringes with the presently available surface conditions.

Table 2 Parameters of the quartz and DCA crystals

	Quartz	DCA
$l_c/\mu\text{m}$	22	0.25
$n(\omega)$	1.532	1.8
$n(2\omega)$	1.547	2.9

From the Maker-fringes, the evaluation of eqn (5) gives the second-order coefficient d_{22} of the DCA crystal to be 330 times that of d_{11} of the quartz crystal. This value corresponds to a 34 times larger response of DCA as compared to urea. We used $d_{11} = 0.3 \text{ pm V}^{-1}$ of quartz in the calculation. Fresnel transmission coefficients for both DCA and quartz also were considered for the correction.

Conclusion

The polar crystals are ascendants of a new generation of highly anisotropic functional materials with perfect polar order. The capabilities of such materials are astounding: the nonlinear optical response of a microcrystalline powder sample of the polar (DecO,Cl)-azine is visible even by the naked eye! The detailed measurements of the DCA crystal shows that its NLO response is 34 times larger than that of urea. Optimization of the beloamphiphile and systematic SAR studies of the polar organic crystals—which are now within reach for the very first time—undoubtedly will further improve the performance of this new class of functional organic materials. We hope that the ideas and concepts will stimulate excitement, interest and engagement in the interdisciplinary field of polar organic materials.

Acknowledgements

This work was supported by the Petroleum Research Fund of the American Chemical Society (27139-AC4) and by the MU Research Council and Board (URC-98-058, URC-99-069, RB #2358).

References

- 1 *Anisotropic Organic Materials-Approaches to Polar Order*, ed. R. Glaser and P. Kaszynski, ACS Symp. Ser., American Chemical Society, Washington, DC, 2001, vol. 798.
- 2 R. Glaser, N. Knotts and H. Wu, *Chemtracts*, 2003, **16**, 443–452.
- 3 R. Glaser, *Acc. Chem. Res.*, submitted.
- 4 S. D. Shoemaker and T. K. Vanderlick, *Biophys. J.*, 2002, **83**, 2007–2014.
- 5 B. Bagchi, *Chem. Rev.*, 2005, **105**, 3197–3219.
- 6 V. Sokolov and V. Mirsky, *Chem. Sens. Biosens.*, 2004, **2**, 255–291.
- 7 G. A. Sim, *Acta Crystallogr.*, 1955, **8**, 833–840.
- 8 M. Masuda and T. Shimizu, *Chem. Commun.*, 2001, 2442–2443.
- 9 R. Glaser, N. Knotts, Z. Wu and C. L. Barnes, *Cryst. Growth Des.*, 2006, **6**, 235–240.
- 10 L. Walz, H. Paulus and W. Haase, *Z. Kristallogr.*, 1987, **180**, 97–121.
- 11 J. Zyss, I. Ledoux, M. Bertault and E. Toupet, *Chem. Phys.*, 1991, **150**, 125–135.
- 12 M. Lewis, Z. Wu and R. Glaser, *Double T-Contacts. Lateral Synthons in the Engineering of Highly Anisotropic Organic Crystals*, ch. 7, in ref. 1.
- 13 D. Steiger, C. Ahlbrandt and R. Glaser, *J. Phys. Chem. B*, 1998, **102**, 4257–4260.
- 14 D. Steiger and R. Glaser, *J. Comput. Chem.*, 2001, **22**, 208–215.
- 15 G. R. Desiraju, *Stimul. Concepts Chem.*, 2000, 293–306.
- 16 R. Glaser and G. S. Chen, *J. Comput. Chem.*, 1998, **19**, 1130–1140.
- 17 M. Lewis and R. Glaser, *J. Org. Chem.*, 2002, **67**, 1441–1447; M. Lewis and R. Glaser, *J. Org. Chem.*, 2002, **67**, 7168.
- 18 R. Glaser, N. Chen, H. Wu, N. Knotts and M. Kaupp, *J. Am. Chem. Soc.*, 2004, **126**, 4412–4419.
- 19 J. A. Williams, *Acc. Chem. Res.*, 1993, **26**, 593–598.
- 20 R. Glaser, M. Lewis and Z. Wu, *J. Mol. Model.*, 2000, **6**, 86–98.
- 21 P. Metrangolo and G. Resnati, *Chem. Eur. J.*, 2001, **7**, 2511–2519.
- 22 G. S. Chen, J. K. Wilbur, C. L. Barnes and R. Glaser, *J. Chem. Soc., Perkin Trans. 2*, 1995, 2311–2317.
- 23 M. Lewis, C. L. Barnes and R. Glaser, *Acta Crystallogr., Sect. C*, 2000, **56**, 393–396.
- 24 M. Lewis, C. L. Barnes and R. Glaser, *J. Chem. Crystallogr.*, 2000, **30**, 489–496.
- 25 N. Knotts, PhD Dissertation, University of Missouri–Columbia, Columbia, Missouri, 2005.
- 26 M. Lewis, Ph.D. Dissertation, University of Missouri–Columbia, Columbia, Missouri, 2001.
- 27 G. S. Chen, M. Anthamatten, C. L. Barnes and R. Glaser, *Angew. Chem.*, 1994, **106**, 1150–1152; G. S. Chen, M. Anthamatten, C. L. Barnes and R. Glaser, *Angew. Chem., Int. Ed. Engl.*, 1994, **33**, 1081–1083.
- 28 G. S. Chen, M. Anthamatten, C. L. Barnes and R. Glaser, *J. Org. Chem.*, 1994, **59**, 4336–4340.
- 29 M. Lewis, C. Barnes and R. Glaser, *J. Chem. Crystallogr.*, 1999, **29**, 1043–1048.
- 30 R. Glaser, G. S. Chen, M. Anthamatten and C. L. Barnes, *J. Chem. Soc., Perkin Trans. 2*, 1995, 1449–1458.
- 31 R. Glaser, G. S. Chen and C. L. Barnes, *J. Org. Chem.*, 1993, **58**, 7446–7455.
- 32 A. R. Katritzky, G. P. Savage, M. Pilarska and Z. Dega-Szafran, *Chem. Scr.*, 1989, **29**, 235–239.
- 33 A. Koziara, K. Turski and A. Zwierzak, *Synthesis*, 1986, 298–301.
- 34 A. Zwierzak and A. Sulewska, *Synthesis*, 1976, 835–837.
- 35 M. Lewis, Z. Wu and R. Glaser, *Arene-Arene Double T-Contacts. Lateral Synthons in the Engineering of Highly Anisotropic Organic Crystals*, ch. 7 in ref. 1.
- 36 D. Beljonne, Z. Shuai, R. H. Friend and J. L. Bredas, *J. Chem. Phys.*, 1995, **102**, 2042–2049.
- 37 J. Cornil, D. A. Santos, X. Crispin, R. Silbey and J. L. Bredas, *J. Am. Chem. Soc.*, 1998, **120**, 1289–1299.
- 38 J. Jerphagnon and S. K. Kurtz, *J. Appl. Phys.*, 1970, **41**, 1667–1681.
- 39 G. T. Kiehne, G. K. Wong and J. B. Ketterson, *J. Appl. Phys.*, 1998, **84**, 5922–5927.
- 40 R. T. Bailey, G. Bourhill, F. R. Cruickshank, D. Pugh, J. N. Sherwood and G. S. Simpson, *J. Appl. Phys.*, 1993, **73**, 1591–1597.
- 41 R. T. Bailey, F. R. Cruickshank, D. Pugh, J. N. Sherwood, G. S. Simpson and S. Wilkie, *J. Appl. Phys.*, 1995, **78**, 1388–1390.
- 42 F. Pan, R. T. Bailey, F. R. Cruickshank, D. Pugh, J. N. Sherwood, G. S. Simpson and S. Wilkie, *J. Appl. Phys.*, 1996, **80**, 4649–4654.
- 43 D. A. Higgins, D. A. Vanden Bout, J. Kerimo and P. F. Barbara, *J. Phys. Chem.*, 1996, **100**, 13794–13803.
- 44 P. M. Lundquist, W. P. Lin, G. K. Wong, M. Razeghi and J. B. Ketterson, *Appl. Phys. Lett.*, 1995, **66**, 1883–1885.
- 45 K. D. Singer and L. A. King, *J. Appl. Phys.*, 1991, **70**, 3215–3222.
- 46 Y. R. Shen, *The Principle of Nonlinear Optics*, Wiley, New York, 1985.
- 47 S. Lochran, R. T. Bailey, F. R. Cruickshank, D. Pugh, J. N. Sherwood, G. S. Simpson, P. J. Langley and J. D. Wallis, *J. Phys. Chem.*, 2000, **104**, 6710–6716.